Journal of Molecular Spectroscopy **202,** 53–58 (2000)
doi:10.1006/jmsp.2000.8111, available online at http://www.idealibrary.com on IDEAL®

Laser-Induced Fluorescence and Fourier Transform Spectroscopy of the $[21.9]^2\Delta_{5/2}$–$X^2\Pi_{3/2}$ (21 910 cm^{-1}) and the $[21.9]^2\Delta_{5/2}$–$[.16]^2\Delta_{5/2}$ (21 750 cm^{-1}) Transitions of NiCl

T. Hirao,* C. Dufour,† B. Pinchemel,‡ and P. F. Bernath*

*Department of Chemistry, University of Waterloo, Waterloo, Ontario, Canada N2L 3G1; †I.E.M.N., UMR CNRS 8520, Université des Sciences et Technologies de Lille, Avenue Poincaré, B.P. 39, 59652, Villeneuve d'Ascq Cedex, France; and ‡Laboratoire de Physique des Lasers, Atomes et Molécules, UMR CNRS 8523, Centre d'Etudes et de Recherches Lasers et Applications, Université des Sciences et Technologies de Lille, 59655, Villeneuve d'Ascq Cedex, France

Received December 2, 1999; in revised form March 14, 2000

The visible spectrum of NiCl consists of a large number of bands. Laser-induced fluorescence experiments have shown that two intense transitions (21 910 and 21 750 cm^{-1}) share a common $[21.9]^2\Delta_{5/2}$ upper electronic state. High-resolution Fourier transform spectroscopy has allowed the rotational analysis of the (0–0), (1–0), and (0–1) bands of the $[21.9]^2\Delta_{5/2}$–$[0.16]^2\Delta_{5/2}$ transition and the (0–0) band of the $[21.9]^2\Delta_{5/2}$–$X^2\Pi_{3/2}$ transition. No fluorescence to a state lower in energy than the $X^2\Pi_{3/2}$ state was observed in our experiments. We believe that we have identified the $^2\Pi_{3/2}$ spin–orbit component of the $X^2\Pi_i$ ground state and the $^2\Delta_{5/2}$ spin–orbit component of the first $A^2\Delta_i$ electronic state.

I. INTRODUCTION

The visible spectrum of NiCl has been known for a long time (*1–4*). It consists of a large number of bands and several attempts have been made to assign these bands in terms of electronic transitions (*1–5*). It is well-known that the open *d* shell of transition metal atoms is generally responsible for the presence of low-lying states in the corresponding diatomic molecules. For example, the isovalent NiF molecule exhibits three electronic states in the first 2500 cm^{-1} above the ground state (*6*). In addition, the vibrational constants of these states are generally similar and can be accidentally almost equal to the intervals between the low-lying electronic states. This can lead to misassignments in both the electronic states and the vibrational structure.

Dispersed laser-induced fluorescence is an efficient way to overcome these difficulties and possibly to enhance weak transitions present in an emission spectrum (*7*). In addition, this technique can be of great help in spectral regions in which the overlapping of bands prevents any analysis (*8*). When applied to NiCl, laser-induced fluorescence showed that the two transitions studied in this paper share a common upper state and helped to ascertain the vibrational assignment. Laser-excitation spectroscopy can be used to obtain high-resolution spectra, but the method is usually time consuming. In contrast, such high-resolution spectra can be easily recorded with a Fourier transform spectrometer, which gives simultaneous coverage in a wide spectral region. In this paper we combine information provided by low-resolution dispersed laser-induced fluorescence with high-resolution spectra supplied by Fourier transform spectroscopy to perform the first rotational analysis of two electronic transitions of NiCl lying at 21 750 and 21 910 cm^{-1}.

II. EXPERIMENTAL DETAILS

The low-resolution fluorescence experiments have been performed in a high-temperature oven (*8*). A sample of nickel was electrically heated in a graphite tube (1-cm internal diameter) at a temperature of about 1300 K under a pressure of 100 Torr of argon. A few Torr of methyl chloride was added to react with the nickel atoms to produce NiCl. The laser beam (200 mW) was provided by a broadband cw dye laser (Coherent 699-01) running with stylbene dye and pumped by 3 W of the UV lines of a Coherent Innova argon ion laser. The laser beam interacts with the molecules along the axis of the graphite tube. The fluorescence signal is then focused on the entrance slit of a spectrometer (Jobin Yvon THR, focal length of 1.5 m). The dispersed light is recorded by a photomultiplier tube with an associated lock-in amplifier and a chart recorder. The laser line is tuned to the most intense bandheads of NiCl in order to record all the fluorescence signals arising from the laser-populated upper electronic state.

The Fourier transform emission spectra were generated by a 2450-MHz microwave discharge of a mixture of $NiCl_2$ (Aldrich, 99.9%) vapor and He buffer gas (5 Torr). The pellet of $NiCl_2$ solid was placed in a quartz tube and heated by a propane torch. A maximum temperature of about 1000°C could be achieved by this method, and it was expected to provide at least 1 Torr of $NiCl_2$ vapor pressure (*9*). The gas mixture was carried to the discharge region by a flow of gas maintained by a rotary pump. About 100 W of microwave power was applied

0022-2852/00 $35.00

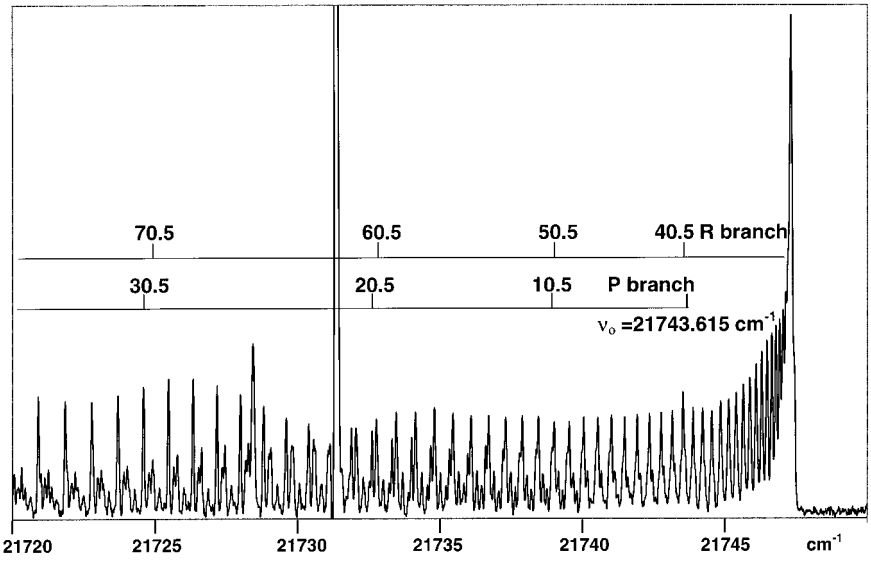

FIG. 1. Part of the $[21.9]^2\Delta_{5/2}$–$[.16]^2\Delta_{5/2}$ 0–0 transition of NiCl.

to a microwave cavity. The emission from the discharge region was focused by a CaF_2 lens into the entrance aperture of the spectrometer.

All emission spectra were recorded with Bruker IFS 120 HR Fourier transform spectrometer at University of Waterloo. The spectrometer was recently modified to record double-sided interferograms (*10*). Because of the use of double-sided interferograms to make the phase correction, the spectral features had an excellent lineshape. Two additional modifications were made to the spectrometer. We made a new emission port in the internal source box and removed a flipping mirror. In this way, molecular emission could be focused directly into the spectrometer with the lens. We also attached the photomultiplier tube detector to the "back parallel exit" of the spectrometer to eliminate all of the mirror reflections associated with the sample and detector compartments. A focusing lens and a small filter compartment were added in front of the photomultiplier tube. In the visible and near UV regions reflection losses from aluminum mirrors are a serious problem. By minimizing the number of mirror reflections, we improved the sensitivity of the spectrometer.

The spectra from 19 800 to 23 600 cm^{-1} were recorded using a quartz beamsplitter. Strong atomic lines of Ni, Cl, and He appeared throughout our spectrum and reduced the signal-to-noise ratio. We used a 450-nm band-pass filter (Corion S40-450) to eliminate as many of the atomic lines as possible. In total, five scans were accumulated in 10 min at a resolution of 0.03 cm^{-1}. The signal-to-noise ratio was about 10, and the typical linewidth was 0.07 cm^{-1}. The accuracy of line positions was estimated to be better than 0.007 cm^{-1}.

The spectrometer was not evacuated, so all line positions were corrected for the refractive index of air (*11, 12*). To convert the line positions to vacuum wavenumbers, we applied the polynomial expression obtained using Edlén's formula (*10*),

$$\Delta = \tilde{\nu}_{ex} - 15\,000, \qquad [1]$$

$$\delta = -6.619702 \times 10^{-3} + 6.7274390 \times 10^{-6} \times \Delta + 7.367955 \times 10^{-10} \times \Delta^2 + 1.864215 \times 10^{-14} \times \Delta^3 + 1.22781 \times 10^{-19} \times \Delta^4 + 2.46704 \times 10^{-24} \times \Delta^5 + 2.8993 \times 10^{-29} \times \Delta^6, \qquad [2]$$

$$\tilde{\nu}_{vac} = \tilde{\nu}_{ex} - \delta, \qquad [3]$$

where $\tilde{\nu}_{ex}$ is the measured spectral position in reciprocal centimeter units in the atmosphere, assuming that the standard internal He–Ne laser emits exactly at 15 798 cm^{-1}, and $\tilde{\nu}_{vac}$ indicates the vacuum wavenumber. Calibration was carried out using Ni atomic lines present in our spectra. Standard line positions were taken from the literature (*13*), and the calibration factor was 1.00000223.

III. DESCRIPTION OF THE BANDS AND VIBRATIONAL ASSIGNMENT

Among the numerous bands observed in the visible spectrum of NiCl, two are obviously more intense and resolved than the others. Both of them are red-degraded. The first one, located at 21 750 cm^{-1}, exhibits an *R* and a *P* branch, while the other (at 21 910 cm^{-1}) has *P*, *Q*, and *R* branches. These bands have

TABLE 1

Bandhead Positions (in cm^{-1}) of the Four Main Isotopomers of the $[21.9]^2\Delta_{5/2}$–$[.16]^2\Delta_{5/2}$ (21 750 cm^{-1}) and the $[21.9]^2\Delta_{5/2}$–$X^2\Pi_{3/2}$ (21 910 cm^{-1}) Transitions of NiCl

v' – v''	^{58}Ni^{35}Cl	^{60}Ni^{35}Cl	^{58}Ni^{37}Cl	^{60}Ni^{37}Cl
$[21.9]^2\Delta_{5/2}$ – $[.16]^2\Delta_{5/2}$ Transition				
0 – 0	21747.3			
1 – 1	21718.5			
2 – 2	21690.5			
0 – 1	21315.7	21318.4	21323.1	21326.0
1 – 2	21290.5	21293.2	21298.2	21301.0
1 – 0	22150.5	22147.9	22143.6	22141.1
2 – 1	22118.2	22116.1		
3 – 2	22086.4			
2 – 0	22550.0			
$[21.9]^2\Delta_{5/2}$ – $X^2\Pi_{3/2}$ Transition				
0 – 0	21910.2			
1 – 1	21890.7			
0 – 1	21488.4	21490.9	21495.5	
1 – 2	21472.3		21479.5	
1 – 0	22312.8	22310.3	22306.0	
2 – 1	22290.2			
3 – 2	22267.7			

been correctly identified as 0–0 bands by Reddy and Rao (*4*) in a vibrational analysis.

Fluorescence experiments were performed to identify transitions sharing a common upper state, in order to build up an energy level diagram of the electronic states of NiCl. We successively tuned the laser to the *R* heads of the transitions at 21 910 and 21 750 cm^1, and we observed that in each case the other transition appeared with enhanced intensity. Most of these experiments were made by observation through the photographic exit of the spectrometer. This allowed the direct observation of the changes in the fluorescence signal induced by scanning the laser. Observation of the 0–1 vibrational bands for each transition, on the basis of previous works (*3–5*), confirmed that the interval of 160 cm^{-1} was not associated with the vibrational structure. It was not out of the question that this splitting was in fact the energy difference between two excited states connected by radiative and/or collisional transfer of population, but the interval of 160 cm^{-1} has been also observed by laser-induced fluorescence experiments carried out on two other transitions (at 24 490 and 24 330 cm^{-1}), so that we can assume that this value (160 cm^{-1}) concerns the lower states of the studied transitions. Laser-induced fluorescence experiments provided a framework to start the high-resolution analysis, which confirmed the hypothesis of a common upper state for the studied transitions.

Natural nickel contains two main isotopes, ^{58}Ni (68%) and ^{60}Ni (26%), and there are two isotopes of chlorine, ^{35}Cl (76%) and ^{37}Cl (24%), resulting in four isotopomers of NiCl. From the study of emission spectra, the identification of several vibrational sequences of the two electronic transitions has been possible. The observation of the *R* heads of the three secondary isotopomers confirmed the vibrational assignment. These bandheads are listed in Table 1. The vibrational parameters derived from *R* bandhead positions are summarized in Table 2.

IV. ROTATIONAL ANALYSIS OF THE 21 910 AND 21 750 cm^{-1} BANDS

Taking into account the fact that the two studied bands share a common upper electronic state, these bands have been simultaneously analyzed. The intense, well-resolved 0–0 band lying at 21 750 cm^{-1} exhibits *R* and *P* branches and can be identified as a $\Delta\Omega = 0$ transition (Fig. 1). No fine structure is evident despite the fact that lines are observed up to $J = 96.5$ in the *R* branch. The second band (21 910 cm^{-1}) is a $\Delta\Omega \neq 0$ transition because of the presence of a strong *Q* branch. This *Q* branch made it easy to determine the band origin and as a consequence the exact *J*-numbering of the rotational lines. Fine structure is easily observed in the *R* branch and it cannot be confused with the lines of the secondary isotopomers because the two sets of lines are of equal intensity. The absence of any fine structure in the 21 750 cm^{-1} transition suggests that the splitting originates in the lower state of the 21 910 cm^{-1} transition. The rotational analysis shows that the evolution of this splitting is proportional to J^3.

In addition, it has been possible to analyze the 0–1 band (21 315 cm^{-1}) and the 1–0 band (22 150 cm^{-1}) of the main isotopomer ^{58}Ni^{35}Cl of the $\Delta\Omega = 0$ transition. For the 0–0 band (21 750 cm^{-1}) of this transition, the very good signal-to-noise ratio allowed the observation of a few *R* lines of the secondary isotopomers ^{60}Ni^{35}Cl and ^{58}Ni^{37}Cl. The position of these lines has been correctly calculated on the basis of the rotational constants of the main isotopomer ^{58}Ni^{35}Cl and the usual expressions based on the ratio of the reduced masses (*14*).

All the lines (listed in Table 3) have been simultaneously

TABLE 2

Equilibrium Parameters (in cm^{-1} unless quoted) for the $[21.9]^2\Delta_{5/2}$, $[.16]^2\Delta_{5/2}$, and $X^2\Pi_{3/2}$ States of NiCl (all uncertainties are 1σ)

State	T_e	ω_e	$\omega_e x_e$	B_e	α_e x 10^4	r_e(Å)
$[21.9]^2\Delta_{5/2}$	21919.90(5)	406.09(3)	1.65(1)	0.17543(1)	9.4(2)	2.0988(1)
$[0.16]^2\Delta_{5/2}$	157.70(5)	435.52(3)	1.90(2)	0.18431(1)	11.2(2)	2.0477(1)
$X^2\Pi_{3/2}$	0	425.63(3)	1.75(2)	[0.18142][a]		[2.0482][b]

[a] B_0 value
[b] r_0 value

TABLE 3

Observed Line Positions (in cm^{-1}) for the $[21.9]^2\Delta_{5/2}$–$[.16]^2\Delta_{5/2}$ (21 750 cm^{-1}) and the $[21.9]^2\Delta_{5/2}$–$X^2\Pi_{3/2}$ (21 910 cm^{-1}) Transitions of NiCl

	0 - 0 band		0 - 1 band		1 - 0 band	
J	P branch	R Branch	P branch	R Branch	P branch	R Branch
3.5			21310.112			
4.5	21741.822		21309.698			
5.5	21741.360		21309.266			
6.5	21740.915		21308.811			
7.5	21740.447		21308.341			
8.5	21739.937		21307.868			
9.5	21739.423		21307.376			
10.5	21738.894		21306.886			
11.5	21738.338		21306.352			
12.5	21737.764		21305.796			
13.5	21737.185		21305.251			
14.5	21736.577		21304.679		22139.694	
15.5	21735.957		21304.079		22139.048	
16.5	21735.318		21303.493		22138.422	
17.5	21734.657		21302.883		22137.721	
18.5	21733.990		21302.252		22136.989	
19.5	21733.298		21301.615		22136.251	
20.5	21732.590		21300.952		22135.545	
21.5	21731.868		21300.256		22134.724	22150.071
22.5	21731.115		21299.572		22133.960	22149.980
23.5	21730.369		21298.858		22133.192	22149.874
24.5	21729.585	21747.097	21298.140		22132.354	22149.763
25.5	21728.792	21746.999	21297.424		22131.520	22149.601
26.5	21727.982	21746.884	21296.645	21315.546	22130.642	22149.445
27.5	21727.159	21746.754	21295.887	21315.490	22129.771	22149.242
28.5	21726.315	21746.606	21295.104	21315.390	22128.868	22149.046
29.5	21725.455	21746.436	21294.322	21315.294	22127.966	22148.825
30.5	21724.577	21746.253	21293.488	21315.166	22127.029	22148.586
31.5	21723.683	21746.054	21292.677	21315.055	22126.060	22148.330
32.5	21722.765	21745.836	21291.824	21314.906	22125.093	22148.044
33.5	21721.832	21745.606	21290.961	21314.745	22124.083	22147.732
34.5	21720.883	21745.352	21290.095	21314.569	22123.092	22147.417
35.5	21719.918	21745.091	21289.199	21314.382	22122.073	22147.121
36.5	21718.937	21744.802	21288.298	21314.175	22121.007	22146.765
37.5	21717.933	21744.496	21287.392	21313.951	22119.943	22146.370
38.5	21716.914	21744.173	21286.454	21313.700	22118.838	22145.970
39.5	21715.885	21743.840	21285.494	21313.467		22145.569
40.5	21714.834	21743.483	21284.544	21313.189	22116.605	22145.128
41.5	21713.762	21743.110	21283.568	21312.910	22115.475	22144.669
42.5	21712.679	21742.722	21282.577	21312.602	22114.329	22144.203
43.5	21711.580	21742.313	21281.578	21312.310	22113.130	22143.706
44.5	21710.456	21741.887	21280.553	21311.993	22111.934	22143.162
45.5	21709.322	21741.446	21279.513	21311.624	22110.732	22142.654
46.5	21708.168	21740.983	21278.453	21311.277	22109.459	22142.090
47.5	21707.001	21740.508	21277.401	21310.900	22108.240	22141.523
48.5	21705.811	21740.010	21276.318	21310.521	22106.953	22140.948
49.5	21704.601	21739.500	21275.220	21310.112	22105.665	22140.343
50.5	21703.384	21738.974	21274.108	21309.698	22104.337	22139.744
51.5	21702.144	21738.424	21272.976	21309.266	22102.995	22139.106
52.5	21700.889	21737.859	21271.835	21308.811	22101.643	22138.422
53.5	21699.616	21737.277	21270.697	21308.341	22100.280	22137.754
54.5	21698.330	21736.682	21269.533	21307.868	22098.892	22137.037
55.5	21697.025	21736.066	21268.337	21307.376	22097.476	22136.305
56.5	21695.703	21735.432	21267.133	21306.886	22096.059	22135.545
57.5	21694.362	21734.786			22094.605	22134.815
58.5	21693.006	21734.121			22093.150	22134.032
59.5	21691.632	21733.441			22091.662	22133.255
60.5	21690.239	21732.737			22090.155	22132.428
61.5	21688.836	21732.021			22088.663	22131.592
62.5	21687.401					22130.763
63.5	21685.971	21730.536				22129.860
64.5	21684.515	21729.746				
65.5	21683.039	21728.980				22128.072
66.5	21681.554	21728.165				22127.122
67.5	21680.036	21727.351				
68.5	21678.521	21726.513				
69.5	21676.987	21725.645				
70.5	21675.424	21724.774				
71.5	21673.844	21723.896				
72.5	21672.260	21722.973				
73.5	21670.666	21722.077				
74.5	21669.039					
75.5	21667.414					
76.5	21665.750					
77.5	21664.074					
78.5	21662.392					
79.5						
80.5	21658.981					
81.5	21657.243					

	0 - 0 band	0 - 1 band	1 - 0 band
J	R branch	R branch	R branch
82.5	21655.500		
83.5	21653.733		
84.5	21651.944		
85.5	21650.154		
86.5	21648.328		
87.5	21646.491		
88.5	21644.653		
89.5	21642.794		
90.5	21640.905		
91.5	21639.002		
92.5			
93.5	21635.169		
94.5	21633.222		
95.5	21631.263		
96.5	21629.290		

J	Q_{ie} branch	Q_{ef} branch	P_{ff} branch	P_{ee} branch	R_{ff} branch	R_{ee} branch
8.5	21904.643	21904.594				
9.5	21904.533	21904.485				
10.5	21904.411	21904.362				
11.5	21904.237	21904.188				
12.5	21904.083	21904.034				
13.5	21903.923	21903.874	21899.194	21899.194		
14.5	21903.757	21903.708	21898.620	21898.620		
15.5	21903.528	21903.479	21898.114	21898.114		
16.5	21903.334	21903.285	21897.524	21897.524		
17.5	21903.100	21903.051	21896.953	21896.953		
18.5	21902.871	21902.822	21896.387	21896.387		
19.5	21902.605	21902.556	21895.771	21895.771		
20.5	21902.344	21902.296	21895.134	21895.134		
21.5	21902.060	21902.011	21894.532	21894.532		
22.5	21901.768	21901.719	21893.884	21893.884		
23.5	21901.475	21901.427				
24.5	21901.158	21901.109	21892.599	21892.599		
25.5	21900.831	21900.782	21891.865	21891.865		
26.5	21900.501	21900.452	21891.234	21891.234		
27.5	21900.138	21900.089	21890.514	21890.514		
28.5	21899.780	21899.731	21889.788	21889.788		
29.5	21899.420	21899.371				
30.5	21899.017	21898.968				
31.5	21898.620	21898.571				
32.5	21898.191	21898.142			21909.951	
33.5	21897.763	21897.714			21909.874	
34.5	21897.322	21897.273			21909.773	
35.5	21896.871	21896.822			21909.670	
36.5	21896.387	21896.338			21909.560	
37.5	21895.905	21895.856			21909.435	
38.5	21895.411	21895.425			21909.301	
39.5	21894.925	21894.937			21909.147	
40.5	21894.370	21894.411			21908.977	21908.880
41.5	21893.860	21893.901			21908.794	21908.689
42.5	21893.291	21893.334			21908.601	21908.486
43.5	21892.752	21892.781			21908.399	21908.277
44.5	21892.160	21892.212			21908.180	21908.060
45.5	21891.583	21891.661			21907.939	21907.822
46.5	21890.996	21891.056			21907.699	21907.578
47.5	21890.379	21890.467			21907.448	21907.307
48.5	21889.765				21907.168	21907.031
49.5	21889.115	21889.220			21906.889	21906.744
50.5	21888.482	21888.578			21906.587	21906.432
51.5	21887.799	21887.909			21906.288	21906.098
52.5	21887.121	21887.267			21905.968	21905.773
53.5	21886.428	21886.557			21905.632	21905.451
54.5	21885.744	21885.907			21905.267	
55.5	21885.008	21885.185			21904.933	
56.5	21884.322	21884.456			21904.533	
57.5	21883.531	21883.726			21904.151	
58.5	21882.808	21882.979			21903.754	
59.5	21882.027	21882.238			21903.334	
60.5	21881.269	21881.464			21902.925	
61.5		21880.680				
62.5	21879.633	21879.884				
63.5	21878.826	21879.061				
64.5	21877.988	21878.246				

TABLE 4
Molecular Constants (in cm^{-1}) for the [21.9]$^2\Delta_{5/2}$, [.16]$^2\Delta_{5/2}$, and $X^2\Pi_{3/2}$ States of NiCl (all uncertainties are 1σ)

State		T_v	B_v	$D_v \times 10^7$	$q_J \times 10^7$
[21.9] $^2\Delta_{5/2}$	v = 1	22308.464(4)	0.174081(10)	1.173(24)	
	v = 0	21905.165(4)	0.1750231(47)	1.180(11)	
[0.16] $^2\Delta_{5/2}$	v = 1	593.701(4)	0.182633(10)	1.265(25)	
	v = 0	161.550(4)	0.1837527(46)	1.311(10)	
X $^2\Pi_{3/2}$	v = 0	0	0.181421(12)	1.172(20)	11.35(25)

fitted. The rovibronic levels of the two excited states (T_0 = 161.5 cm^{-1} and T_0 = 21 905.1 cm^{-1}) are described by the expression (*14*):

$$T = T_v + B_v J(J+1) - D_v J^2(J+1)^2.$$

The expression for the lower state in which a splitting is observed is (*14*)

$$T = T_v + B_v J(J+1) - D_v J^2(J+1)^2 \pm 0.5 q_J J(J+1)(J+0.5),$$

where the *plus* and *minus* signs refer to the *e* and *f* rotational levels, respectively. The derived constants are listed in Table 4 and the equilibrium constants, if they could be calculated, in Table 2. Note that q_J was assumed to be positive.

V. DISCUSSION

Taking into account the large number of bands observed in the visible spectrum of NiCl, there is no doubt that the study of the electronic transitions will be a difficult task. Up until now, the study of the isovalent NiF molecule (*7*, and references therein) includes 30 electronic transitions linking 13 electronic spin–orbit components for the doublet states. As a consequence we must consider our work as a first step in the study of NiCl.

Attempts to ascertain the symmetry of the electronic states involved in the two analyzed transitions are somewhat puzzling. We observe that no $^2\Sigma$ state is involved in any of the two transitions because the $\Delta\Omega \neq 0$ transition (21 910 cm^{-1}) would be a $^2\Sigma$–$^2\Pi$ or a $^2\Pi$–$^2\Sigma$ transition. In this case the rotational pattern would not correspond to the experimentally observed one, unless the $^2\Pi$ state obeys perfect Hund's case (b) coupling (*14*). Let us now suppose that only $^2\Pi$ and $^2\Delta$ states are involved in the two transitions, which cannot be expected to be forbidden if we consider their intensities. As noted in Section IV, a splitting is observed in the 0–0 band of the 21 910 cm^{-1} transition, which can be interpreted as a Λ-doubling. The splitting is proportional to J^3, characteristic of a spin–orbit component in which the projection of the total electronic angular momentum Ω is equal to 3/2 (*14*), i.e., either a $^2\Pi_{3/2}$ or a $^2\Delta_{3/2}$ spin component.

Two schemes can then be suggested: (i) the upper state is a $^2\Delta_{5/2}$ state and the transitions are $^2\Delta_{5/2}$–$^2\Pi_{3/2}$ (21 910 cm^{-1}) and $^2\Delta_{5/2}$–$^2\Delta_{5/2}$ (21 750 cm^{-1}) or (ii) the upper state is a $^2\Pi_{1/2}$ component and the observed transitions are then $^2\Pi_{1/2}$–$^2\Delta_{3/2}$ (21 910 cm^{-1}) and $^2\Pi_{1/2}$–$^2\Pi_{1/2}$ (21 750 cm^{-1}). It is obvious that the second hypothesis is less consistent with the data than the first one because the presence of a $^2\Pi_{1/2}$ spin component should lead to the observation of a splitting of the lines in the 21 750 cm^{-1} transition. The first hypothesis agrees with the observation of a splitting proportional to J^3 in the lower $^2\Pi_{3/2}$ state of the 21 910 cm^{-1} transition and with the absence of any splitting in the 21 750 cm^{-1} transition as expected for a $^2\Delta_{5/2}$–$^2\Delta_{5/2}$ transition.

In the case of NiF three electronic states ($^2\Pi_i$, $^2\Delta_i$, and $^2\Sigma^+$) are observed in the first 2500 cm^{-1} above the $^2\Pi_{3/2}$ ground state. We can suppose that NiCl will be similar and that the lower spin–orbit components of the studied transitions belong to the lowest $^2\Pi_i$ and $^2\Delta_i$ states. The fluorescence experiments are enlightening. We have detected no fluorescence signal on the higher wavenumber side of the 21 910 cm^{-1} band when the laser line was tuned in resonance. Assuming that the upper state of this transition is a $^2\Delta_{5/2}$ state, then no other $^2\Delta_{5/2}$ or $^2\Pi_{3/2}$ spin–orbit components can lie at a lower energy than that of the lowest state involved in the two studied transitions, but this does not eliminate the possible presence of a $^2\Sigma$ ground state. However, fluorescence experiments have been carried out on other electronic transitions which have a common lower state with the 21 910 cm^{-1} transition and they never led to the observation of a fluorescence signal to higher wavenumbers than the probed transition. Despite the fact that up until now none of these transitions have been rotationally analyzed, we can suppose that a $^2\Pi_{3/2}$ upper state is involved in at least one of the probed transitions, which would give rise to fluorescence of an allowed $^2\Pi_{3/2}$–$^2\Sigma$ transition. All these fluorescence experiments lead to the observation of bands redder than the probed transition and we can conclude that no $^2\Sigma$ state lies at a lower energy than that of the $^2\Pi_{3/2}$ state involved in the $^2\Delta_{5/2}$–$^2\Pi_{3/2}$ transition (21 910 cm^{-1}). The $X^2\Pi_{3/2}$ state is thus the ground state of NiCl.

VI. CONCLUSION

The analysis of two electronic transitions observed in the visible spectrum of NiCl led to the determination of the vibrational and rotational parameters of three electronic states. Dispersed laser-induced fluorescence experiments suggest that the lower states of these transitions, which share a common upper state, are the $^2\Pi_{3/2}$ and the $^2\Delta_{5/2}$ spin–orbit components of the ground $^2\Pi_i$ state and the first excited $^2\Delta_i$ electronic state of NiCl. From a comparison with the isovalent NiF molecule (*6–8*), which has three low-lying electronic states ($X^2\Pi_i$, $^2\Sigma$, and $^2\Delta_i$) in the first 2500 cm^{-1}, we suggest that the transitions studied in our work are the [21.9]$^2\Delta_{5/2}$–$X^2\Pi_{3/2}$ (21 910 cm^{-1})

and the $[21.9]^2\Delta_{5/2}$–$[0.16]^2\Delta_{5/2}$ (21 750 cm^{-1}) transitions sharing a common upper state. The determination of the relative positions of the two lower states, $X^2\Pi_{3/2}$ and $[0.16]^2\Delta_{5/2}$, and the measurements of their vibrational and rotational parameters, will be of great help in the study of the numerous other electronic transitions observed in the visible and the near-infrared spectral regions. This work is a good example of the complementarity of laser-induced fluorescence spectroscopy and Fourier transform spectroscopy for the analysis of spectra of transition metal-containing molecules that often have several low-lying electronic states.

ACKNOWLEDGMENTS

The Centre d'Etudes et de Recherches Lasers et Applications is supported by the Ministère Chargé de la Recherche, the Région Nord-Pas de Calais, and the Fond Européen de Développement Economique des Régions. This work was supported by the Natural Sciences and Engineering Research Council of Canada (NSERC). Acknowledgment is also made to the Petroleum Research Fund for partial support.

REFERENCES

1. P. Mesnage, *C. R. Acad. Sci.* **200,** 2072–2074 (1935).
2. K. R. More, *Phys. Rev.* **54,** 122–125 (1938).
3. V. G. Krishnamurty, *Indian J. Phys.* **26,** 207–225 (1952).
4. S. P. Reddy and P. T. Rao, *Proc. Phys. Soc.* **75,** 275–282 (1960).
5. R. Gopal and M. M. Joshi, *Indian J. Pure Appl. Phys.* **20,** 280–283 (1982).
6. C. Dufour, I. Hikmet, and B. Pinchemel, *J. Mol. Spectrosc.* **165,** 398–405 (1994).
7. C. Focsa, C. Dufour, and B. Pinchemel, *J. Mol. Spectrosc.* **182,** 65–71 (1997).
8. A. Bouddou, C. Dufour, and B. Pinchemel, *J. Mol. Spectrosc.* **168,** 477–482 (1994).
9. O. Knacke, O. Kubaschewski, and K. Hesselmann, "Thermochemical Properties of Inorganic Substances," 2nd ed., Springer-Verlag, Berlin/New York, 1991.
10. T. Hirao, B. Pinchemel, and P. F. Bernath, *J. Mol. Spectrosc.*, in press.
11. B. Edlén, *Metrologia* **2,** 71–80 (1966).
12. K. P. Birch and M. J. Downs, *Metrologia* **30,** 155–162 (1993).
13. G. Norlén, *Phys. Scr.* **8,** 249–268 (1973).
14. G. Herzberg, "Spectra of Diatomic Molecules," Van Nostrand, Princeton, 1950.